

Influence of arc oscillation frequencies on the surface of DED-Arc manufactured Ti-6Al-4V structures regarding the specific energy consumption

Hannes Zapf¹ · Robert Lau¹ · Ingomar Kelbassa¹ · Claus Emmelmann²

¹ Fraunhofer IAPT, 21029 Hamburg

² Technische Universität Hamburg, 21073 Hamburg

https://doi.org/10.58134/fh-aachen-rte_2024_007

Abstract

Directed energy deposition based on gas metal arc welding (DED-Arc) is increasingly used for large or coarse near-net-shape structures. Also known as wire arc additive manufacturing (WAAM), DED-Arc produces additive structures, which have a large surface roughness or waviness compared to other additive processes. This results in a large machining allowance, especially at high build rates. In order to improve this surface quality, this study investigated the relation between the oscillation frequency of this arc process on the resulting surface of a Ti-6Al-4V structure. Therefore, multi-layer single pass tracks which perform a sinus like path are used. The surface improvement was then compared to the additional energy required by the robot due to increased oscillation speed and evaluated using the specific energy consumption (SEC). In a first step, several walls were manufactured at maximum wire feed of the system. Here, only the oscillation frequency (OF) was varied in order to obtain the same energy per unit length for all test structures and to ensure comparability. By increasing the OF from 1 to 4.5Hz, a significant improvement in the surface was initially achieved and a proportional relationship was observed. This is also linked to an improvement in the buy-to-fly-ratio (BTF) and ultimately the carbon footprint, since less volume has to be machined due to lower surface waviness. By increasing the OF and thus increasing the welding torch speed and acceleration, a higher energy requirement from the robot system was determined in a second step. In a comparison, it was then shown that the additional robot energy leads to a reduced machining allowance thanks to the resulting better surface. But in total, this results in a lower SEC for a demonstrator structure, since the additional robot energy is a magnitude lower, than the energy input of material savings.

Keywords WAAM · DED-Arc Surface quality Specific energy consumption GMAW Ti-6Al-4V Oscillation frequency

1. Introduction and motivation

Additive manufacturing based on DED-Arc and arc welding technologies is now technologically mature enough to be used as a rapid manufacturing process and is being used for the first time in series production of structural components for the aerospace industry [1]. The DED-Arc process has great potential to quickly establish itself in the industry due to its low component costs, simple safety regulations (e.g. no need for laser protection) compared to DED-LB or DED-EB, while offering at the same time also high build-up rates for a near-net-shape production [2].

On top of that DED-Arc processes have the potential to be more environmentally friendly compared to other conventional manufacturing, such as machining [3]. Life cycle assessment (LCA) studies focused on DED-Arc were carried out in [3–8]. In comparison to the machining option, the BTF ratio (or the reciprocal

definition, solid-to-cavity ratio) of the part has crucial role, since it describes how much material stays within the final part [9]. Using a near-net shape approach in DED-Arc, favorable low BTF ratios result in a lower energy demands along the material processing and manufacturing routes. Especially for titanium alloys, the primary material production has a large impact on the overall energy demand [5, 7]. A further optimization of the BTF in titanium parts manufactured with DED-Arc and a machining finishing can lead to lower energy consumptions. This is the case, if the material savings have larger impact than potential higher energy consumptions during the DED-Arc process.


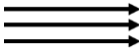


The aim of additive manufacturing is basically to produce functional parts with a surface that requires no or minimal post-processing. Wire-based processes, with their high build-up rates, particularly result in poorer surface finish compared to powder-based processes such as PBF-LB/M or PBF-EB/M [10–12]. Therefore, the

objective is to minimize the machining allowance by optimizing the surface and accuracy, which have a significant influence on the quality of DED-Arc/Ti-6Al-4V components [11].

In principle, many studies focus on improving the surface quality, for which they present mathematical models for finding optimum distances between the weld beads, for example presented in [13–16]. However, these usually apply to the arrangement of individual tracks on a plane or are tailored for steel materials, rendering them inapplicable to the present case.

For the surface and component quality, the process strategy or path planning of how a weld bead is deposited is much more important [17]. This can involve multiple individual tracks or an oscillating movement, for example. Table 1 summarizes different strategies of liquid material deposition on the substrate or on an already built-up layer. It is shown that Ti-6Al-4V can be deposited in a wide variety of ways using DED-Arc and that a basic distinction can be made between oscillating movement strategies (OMS) and non-oscillating movement strategies (NOMS). If one compares the sources mentioned in Table 1 for NOMS with OMS, it is noticeable that OMS produces a significantly better and more uniform surface. On the other hand, NOMS lead to larger surface notches or depressions. This can be explained by the rather unsteady behavior of the liquid titanium, resulting in very highly built-up weld beads with a tendency towards small wetting angles due to the high surface tension, as illustrated in [18]. In contrast, more influence can be applied on the melt by OMS and by utilizing the arc pressure. Moreover, OMS lead to shorter cooling times, as indicated in [19]. This results in broad layers of individual α -colony variations at the β -grain boundaries and thus fundamentally a coarser microstructure than with NOMS. However, the wider layers lead to more resistance to crack growth, which in turn is assessed positively [19].

Table 1: Deposition strategies for DED-Arc of Ti-6Al-4V based on gas metal arc welding (GMAW).

Deposition strategy		References
Non-oscillating movements	Single pass 	[20–22]
	Multi pass 	
Oscillating movements	Meander 	[11, 23–25]
	Wavelike 	

A special consideration of the oscillating parameters resulting from the oscillating motion (e.g. frequency, amplitude, speeds in different spatial directions) has not

been described in detail yet. That is why this paper investigates the potential to lower the BTF of Ti-6Al-4V parts with different OF during the DED-Arc process and contrast the involved robot and part energy consumptions to develop a less energy intensive and more sustainable process route.

2. Method and material

To achieve the above-mentioned objective, an empirical approach was chosen. The DED-Arc -manufactured walls with the dimensions 140 x 115 x 15 [WxHxD] are manufactured with a wire feed speed of 12 m/min, a welding speed of 190 mm/min and an oscillating amplitude of 6 mm. The movement was sinusoidal from the start to the end point, which is a standard oscillating weld path method of the used robot system. This has the advantage of reduced programming effort, shorter programs and more consistent speeds in comparison to pure meander travel. Figure 1 shows the OMS used in more detail. A dwell time is also programmed into the outer areas, resulting in an approximate meandering course. The OF now indicates how quickly and at what angle the arc oscillated to the other side. The OF was varied from 1 Hz to 4.5 Hz, while the other influencing variables remained constant for better comparability. For values smaller than 1 Hz, there would be too much material deposited in the center which leads to an unfavorable height-width-ratio with a triangle-like cross section area. For values bigger than 4.5 Hz, on the one hand the seam starts splitting off in the middle, because the movements speeds became too high and no continuous deposition can be achieved, see annex. On the other hand, the used robot system cannot reach values much higher, than 5 Hz. So, the selected parameter range marked the process limits.

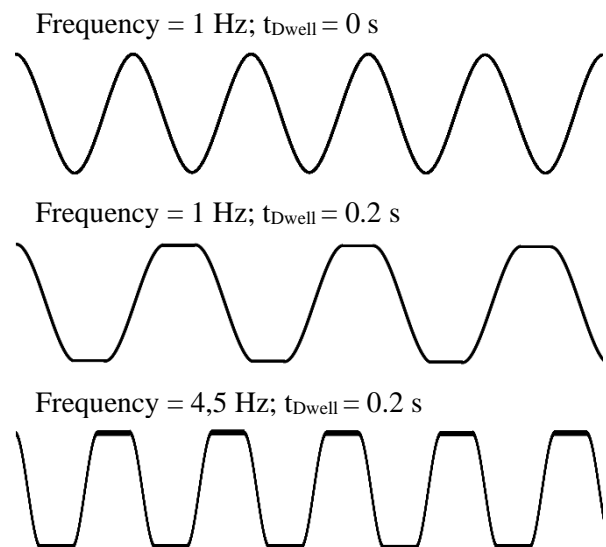


Figure 1: Principle drawing of changing the tool path with OMS as a function of dwell time and frequency.

The machine setup consisted of a FANUC M710iC-50 robot as a handling system, a Fronius TPSi 400 power source with push-pull torch and a protective gas chamber flooded with argon 4.6, see Figure 2. The substrate consisted of sheet metal strips made of Ti-6Al-4V measuring 250 x 50 x 10 mm, onto which the corresponding walls were welded. The feedstock material was a 1.2 mm wire made of Ti-6Al-4V from Böhler Welding and argon 4.6 with a flow rate of 10 l/min was also used as the shielding gas fed through the torch nozzle. The DED-Arc process used was based on the GMAW and utilized the Cold Metal Transfer process variant from Fronius.

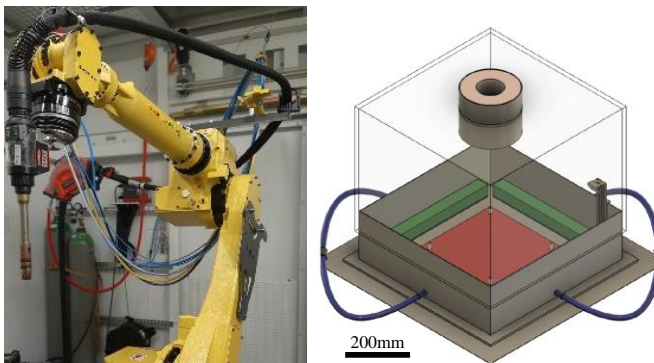


Figure 2: FANUC robot and protective gas chamber used for the described test procedure.

When welding the walls, a constant intermediate layer temperature of 200 °C was ensured. Cooling to this temperature was achieved by free convection in the argon atmosphere and heat conduction into the substrate plate and clamping system. The substrate plate was not actively cooled. The time to reach the temperature increased with increasing layer height from a few seconds up to an order of magnitude of ~15min. Furthermore, the argon atmosphere was continuously monitored for residual oxygen content. The DED-Arc process started at a residual oxygen content of 100 ppm and remained constant for the duration of the build job ± 100 ppm.

Each wall was welded individually in the gas chamber to avoid any possible additional heat influences from other welds. The 30 layers of each wall were always welded in the same direction, resulting in a uniform appearance of the wall.

The surface was measured using a Keyence VR 6200 profile microscope, which emits strip light at an angle of 55 ° to the measuring surface and is detected by a camera at 90 ° to the surface. To detect the primary profile, a 20 mm wide strip from the top edge of the substrate to the second last layer of the printed walls was recorded. Above the second last layer, the wall has a semi-circular cross-section and would falsify the measurement results for the surface, so these were not considered. A

measurement consisted of 63 single pictures using a 40x magnification and micro camera, which are compiled afterwards, see Figure 3. As the ends of the substrate have warped, the measurement was carried out in the center of the substrate to avoid measuring any inclined layers. The overview images of the entire wall in Figure 4 were taken with 12x magnification and a macro camera.

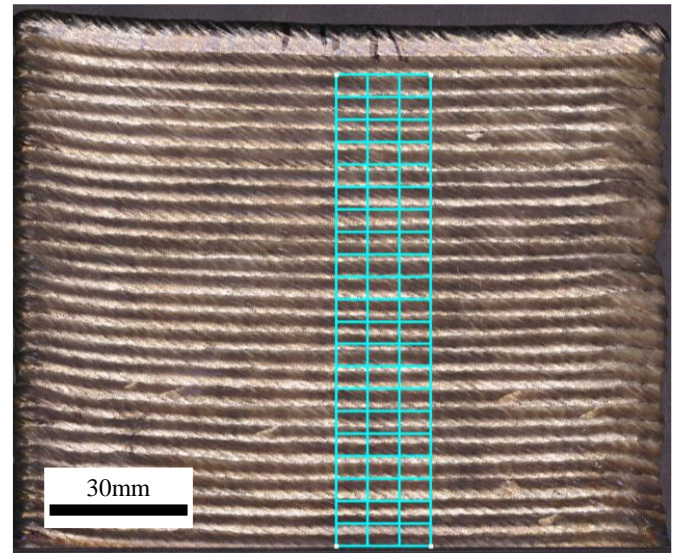


Figure 3: 140 mm long DED-Arc produced wall with representation of the measured surface area to determine the surface properties from Table 2; each rectangle represents a measured single area.

3. Results & discussion

In this chapter, the results for the additively manufactured walls are discussed and a distinction is made between the surface properties and the SEC.

3.1. Surface properties

Figure 4 gives a visual impression of the manufactured walls with different OFs, also, two cross section areas from preliminary tests are shown in the annex. For better comparability, all illustrations are based on the same color scale. The height differences shown are 500% bigger in order to make the differences more visible. In principle, these images already show the effect of the improving surface with increasing OF. For example, the height differences on the wall with 1 Hz extend over the entire scale range from -1.15 mm to + 1.1 mm. In contrast, at 4.5 Hz only the scale range of approx. ± 0.4 mm is reached. However, the differences between 2.5 Hz and 4.5 Hz are no longer noticeable when simply looking at this height specifications. Although there are larger areas with a reddish color at 2.5 Hz, the main difference is the finer rippling at 4.5 Hz, which can be

seen by the aforementioned amplification of the differences. At 1 Hz, the rippling is again much more pronounced and already makes it clear that a larger proportion of material can be found here.

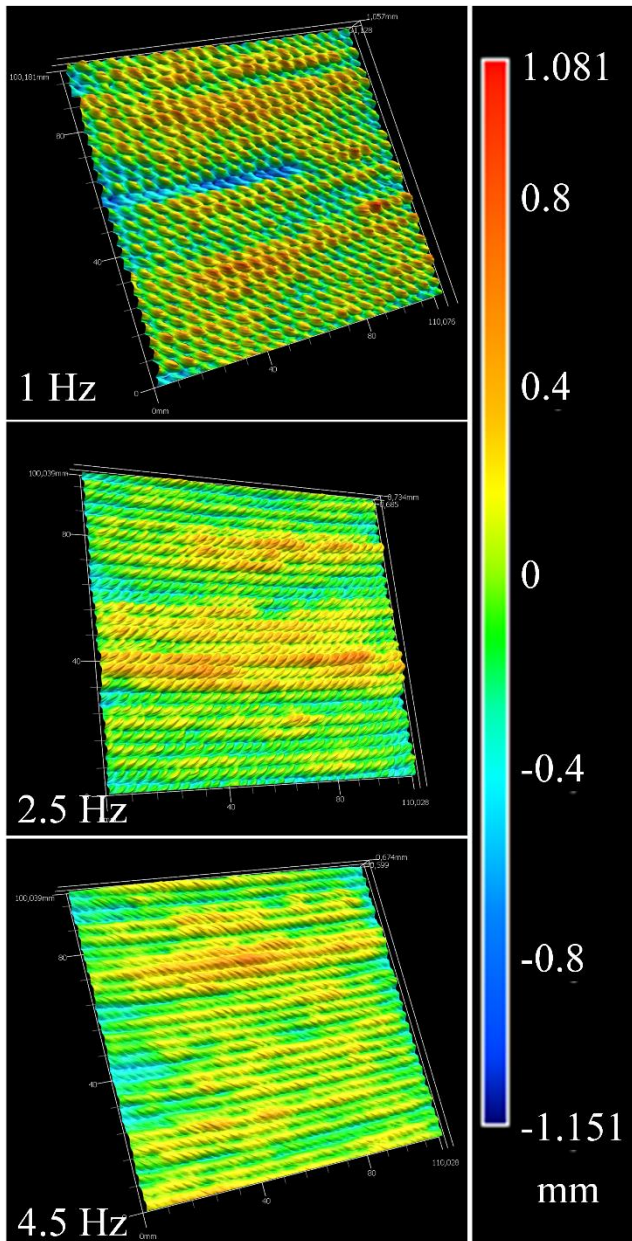


Figure 4: 3D surface of the manufactured wall structures with color highlighting of height differences and visible differences in the surface rippling.

The measured data obtained from the high magnification measurement (Figure 3) were evaluated in the next step and the results are summarized in Table 2. The results are differentiated according to the primary, waviness and roughness profile on the one hand, and according to horizontal and vertical measurement orientation on the other hand. Each specified measured value from Table 2 in the horizontal direction consist of 20 parallel individual lines with a spacing of 1 mm. In the vertical direction, the values consist of 61 parallel individual

lines, which corresponds to the maximum possible number in the evaluation software. The distance between the measurement lines in the horizontal direction is 1.75 mm. This high number and small spacing of the measuring lines ensures that the entire measuring range can be recorded and considered over several layers or over several oscillating movements respectively.

The primary profile P_z corresponds to the initial surface profile. Basically, the aim is to achieve a better BTF or to machine less. The primary profile is therefore the most important, as the entire profile is considered here without filtering a long or short wavelength component or cutting off entry and exit areas and is decisive for the description of the volume to be machined. The waviness and roughness profile can be used to gain a better process understanding and helps to assess the applicability of non-destructive testing processes such as ultrasonic testing. Consideration of the different measurement orientations also helps to describe the process. That means, the measurement in the vertical direction is mainly influenced by the transition of the superimposed layers. In contrast, the horizontal measurement direction describes the oscillating movement within a layer in the welding direction.

The results for the primary profile show a predominantly uniform correlation and change in the primary profile across both measurement orientations over the range of values examined. The average values as well as the maximum and minimum values and the standard deviations decrease as the oscillation frequency increases. For example, the average height of the primary profile in the horizontal direction is 603.5 μm at 1 Hz, 282.6 μm at 2.5 Hz and 187.7 μm at 4.5 Hz. The same picture can be seen when looking at the vertical measurements, but with larger absolute values. Between 1 Hz and 2.5 Hz there is a large jump with a reduction in the average value from 1282 μm to 867.8 μm . With a further increase to 4.5 Hz, the average profile depth only drops by approx. 70 μm to 791.7 μm . The relationship should therefore not be regarded as linear, but rather the reductions in profile depths continue to decrease with increasing oscillation frequency and probably approach a minimum value. The same trends can also be seen for the maximum and minimum values in both measurement directions. Only when looking at the standard deviations a slightly different picture emerges. At 1 Hz, the standard deviation in the vertical direction is 71.6 μm , then rises to 89.4 μm at 2.5 Hz and falls to 87.7 μm at 4.5 Hz. For the vertical direction, oscillation at 1 Hz results in the most uniform primary profile. In the horizontal direction, the previously described trend is again evident: the higher the oscillation frequency, the smaller the standard deviation.

Smaller values for describing the profiles can be classified as fundamentally positive, as they show that the difference between profile peaks and valleys decreases. This makes the surface smoother and ultimately reduces the machining volume.

To determine the roughness and waviness profile, a λ_c -value of 8 was chosen to filter the short- and long-wave components of the primary profile [26]. The results of W_z and R_z are basically similar to the primary profile P_z , although the absolute and relative differences between the measured values are different.

Table 2: Results of the surface measurement in horizontal and vertical measurement direction as averaged values z and arithmetic values a .

Primary profile	Oscillation frequency	P_z horizontal [μm]				P_z vertical [μm]			
		Average	Max	Min	St.dev.	Average	Max	Min	St.dev.
	1 Hz	603.5	1064.6	303.2	167.3	1282.4	1395.3	1127.6	71.6
	2.5 Hz	282.6	638.6	142.7	94.3	867.8	1060.3	741.6	89.4
	4.5 Hz	187.8	344.3	64.5	66.2	791.7	990.2	659.0	87.7

Waviness profile	Oscillation frequency	W_z horizontal [μm]				W_z vertical [μm]			
		Average	Max	Min	St.dev.	Average	Max	Min	St.dev.
	1 Hz	153.1	305.7	61.0	60.0	728.8	920.1	605.2	79.7
	2.5 Hz	97.3	318.8	14.1	64.2	522.8	682.2	425.8	74.0
	4.5 Hz	74.4	243.0	13.3	46.6	511.4	703.2	439.4	72.4

Roughness profile	Oscillation frequency	R_z horizontal [μm]				R_z vertical [μm]			
		Average	Max	Min	St.dev.	Average	Max	Min	St.dev.
	1 Hz	373.9	687.5	125.2	118.3	489.2	607.9	335.9	86.6
	2.5 Hz	142.3	258.0	60.3	45.3	325.9	359.3	282.6	25.2
	4.5 Hz	74.0	139.5	39.4	19.8	270.8	298.9	237.5	17.5

Primary profile	Oscillation frequency	P_a horizontal [μm]				P_a vertical [μm]			
		Average	Max	Min	St.dev.	Average	Max	Min	St.dev.
	1 Hz	132.6	209.6	61.4	40.2	202.4	228.4	172.2	15.2
	2.5 Hz	60.1	161.5	25.0	25.7	157.1	182.0	133.1	14.0
	4.5 Hz	40.3	96.2	13.0	18.6	117.8	130.5	112.2	3.9

Waviness profile	Oscillation frequency	W_a horizontal [μm]				W_a vertical [μm]			
		Average	Max	Min	St.dev.	Average	Max	Min	St.dev.
	1 Hz	48.4	102.2	17.4	21.0	145.8	195.1	120.3	18.9
	2.5 Hz	34.5	107.1	3.4	20.6	134.6	157.9	116.0	13.1
	4.5 Hz	27.3	83.6	2.8	16.1	86.1	95.1	81.7	3.2

Roughness profile	Oscillation frequency	R_a horizontal [μm]				R_a vertical [μm]			
		Average	Max	Min	St.dev.	Average	Max	Min	St.dev.
	1 Hz	97.0	173.8	25.0	34.7	115.7	147.4	74.7	24.3
	2.5 Hz	33.3	55.6	13.2	11.9	71.7	84.7	57.9	8.2
	4.5 Hz	15.3	25.2	8.2	4.1	65.2	69.1	61.3	2.0

However, the roughness profile also shows a strong positive effect with an improvement in the average value for R_z in the horizontal measurement direction from

373.9 μm at 1 Hz to 74 μm at 4.5 Hz. In the vertical direction, the improvement from 1 Hz to 4.5 Hz is approx. 220 μm to $R_z=270\mu\text{m}$. In addition, by looking at the standard deviation, it can also be shown that the results and thus the surface also become significantly more uniform and fluctuate less strongly. For example, the standard deviation drops from 118 μm at 1 Hz to approx. 20 μm at 4.5 Hz in the horizontal measurement direction and even from 86 μm to 17.5 μm in the vertical direction. This development can also be seen as positive, as a more uniform surface offers less potential for vibrations during machining due to different depths of engagement.

Furthermore, it can be seen that the values for the horizontal measurement direction are generally smaller than those for a vertical measurement. Accordingly, the layer structure and its optimization in the vertical direction is more important for the surface quality and a smaller BTF than the surface within a layer.

In a further measurement, the distance between the profile-typical valleys was analyzed in order to obtain measured values for the actual layer height and rippling. Figure 5 shows an example of such a measurement for 2.5 Hz, in which the deepest points in the profile were determined and their distance from each other measured, see Table 3. In principle, the average layer height is at the same level for all OFs and the differences are only in the tenths or hundredths range. However, it can be seen that the standard deviation decreases from 0.67 to 0.41 mm with increasing OF, which means that at 4.5 Hz a more uniform layer build-up takes place.

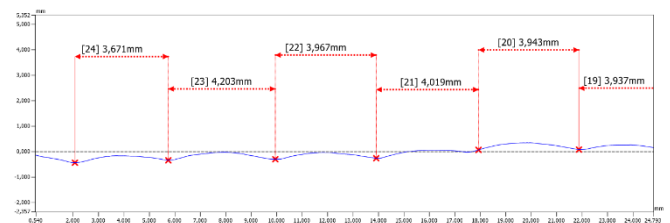


Figure 5: Exemplary measurement of the profile valleys at 2.5 Hz in vertical direction to determine the achieved layer height.

This was also repeated for the vertical direction, see Table 4. Here you can see that the distance between the oscillation cycles (DOC) becomes significantly smaller with increasing OF, which results in finer rippling. However, it can be seen that the standard deviation behaves in the opposite way and increases significantly from 0.181 at 1 Hz to 0.348 at 4.5 Hz. However, it should be noted that the analyzed width was only 20 mm, see chapter 2, so there are only three values at 1 Hz, but 7 at 4.5 Hz, which could change the overall picture to some degrees.

Table 3: Resulting average layer height when measuring profile valleys in vertical direction.

	Layer height at 1 Hz [mm]	Layer height at 2.5 Hz [mm]	Layer height at 4.5 Hz [mm]
Average	3.943	3.955	3.882
Max	5.506	4.677	4.470
Min	2.694	3.078	3.019
St. dev.	0.669	0.441	0.412

Table 4: Resulting distance between oscillating cycles when measuring profile valleys in horizontal direction.

	DOC at 1 Hz [mm]	DOC at 2.5 Hz [mm]	DOC 4.5 Hz [mm]
Average	5.397	3.398	2.677
Max	5.624	3.878	3.286
Min	5.180	3.019	2.338
St. dev.	0.181	0.329	0.348

The effect of the better surface profiles described above is also reflected in the values of the subsequent chip volume. This value describes the volume of all measured profile peaks that must be machined in order to produce a smooth core wall. Therefore, another wall measurement of a 110 mm wide and 100 mm high area was used for this purpose, thus excluding two times a 15 mm wide area around the start and end points. This results in the values of Table 5. For simplification, it was assumed that the front and back were identical and the values could be doubled. Accordingly, the volume to be machined for a wall manufactured with 1 Hz oscillation frequency is 24.8 cm³, which is almost twice as large as for 4.5 Hz at 12.8 cm³. Here too, it can be seen that the differences in the values between 1 Hz and 2.5 Hz are the greatest. The jump here is almost 64 %. The increase to 4.5 Hz also brings a further improvement, but the relative improvement is only 17 % with almost doubled OF. These values form the basis for the calculations for SEC in the following chapter.

Table 5: Measured chip volume for the walls produced with different oscillating frequencies.

OF [Hz]	Chip volume for one wall side [mm ³]	Chip volume for both wall sides [mm ³]
1	12,420.1	24,840.1
2.5	7,559.5	15,119.0
4.5	6,435.6	12,871.1

3.2. Specific energy consumption

The developed process strategy with a higher oscillation frequency results in a reduced machining allowance. The results given by the comparison of the surface profile (chapter 3.1) are analysed as followed in terms of energy consumptions to be able to quantify the impact in a potential LCA. An extensive and consistent LCA (e.g. in a cradle-to-gate approach) is not performed in this study. Since the framing conditions and process parameters are constant for the different oscillation frequencies, only the varying factors are compared. Firstly, the energy consumption for the robot-based process handling is recorded to quantify the higher moving effort for the increasing oscillating frequencies. Secondly, the energy consumptions for the material processing steps are analysed to quantify the effect for the savings in material. The functional unit for the comparison is the defined wall structure.

The values for the energy consumption of the robot system are measured on a test track of 190 mm length with arc off and the above-mentioned welding speed of 190 mm/min. This made it possible to obtain the pure power consumption in the movement of the robot, without influences from positioning movements or standstill times. These values are converted to the 110 mm measured track length of the wall structure. For each oscillation frequency the values are summarized in Table 6. Thereby, only the welding time of approx. 17 minutes for each whole wall is considered and idle times are neglected. The comparison of the 1 Hz to the 4.5 Hz oscillation frequency shows an increase of 1.1 % in the energy consumption, which relates to a total increase of 6.5 kJ.

Table 6: Energy consumption of the robot for welding time of each wall.

OF [Hz]	Energy consumption [kWh]	Increase relative to 1 Hz [%]	Increase relative to 1 Hz [kJ]
1	0.1613	-	-
2.5	0.1626	0.8	4.7
4.5	0.1631	1.1	6.5

For the assessment of the material processing steps, only the energy consumption is considered and emissions, wastes and consumables are neglected. Priarone et al. present a methodology to compare the environmental performance of DED-Arc processes [9]. Accordingly, the main phases during the material processing of titanium wire, the primary material production, the hot rolling and the wire drawing are part of this simplified assessment. To be able to quantify the phases with values for the SEC, a literature review is carried out. All

values are converted to MJ/kg and the mean value of each phase is used for a refined comparison. The primary material production has by far the highest impact (617 MJ/kg), followed by hot rolling (16 MJ/kg) and wire drawing (8.7 MJ/kg), see Table 7.

Table 7: Specific energy consumption for the material processing steps.

Phase	SEC [MJ/kg]	Reference
Primary material production	556.2	[CES Selector2017, Update 1, version 17.2.0 (Granta Design Limited, the UK).] reported by [5]
	685	[27]
	475.5	[28]
	556.2	[29]
	973.33	[30]
	457.2	[31]
Mean value	617.2	
Hot rolling	16.8	[CES Selector2017, Update 1, version 17.2.0 (Granta Design Limited, the UK).] reported by [5]
	15.1	[31]
Mean value	16.0	
Wire drawing	8.13	[CES Selector2017, Update 1, version 17.2.0 (Granta Design Limited, the UK).] reported by [5]
	9.36	[31]
Mean value	8.7	

The calculation of the machining volume to receive the core wall structure for each oscillation frequency is based on the surface measurement (see section 3.1) and density of 4.43 g/cm³ for titanium, see Table 8. The chipping volume for both sides of the wall structure reduces from 110 g for 1 Hz oscillation frequency to 57 g for 4.5 Hz. Thus, the optimized process strategy results in a material saving of 53 g for the wall structure. Multiplied with the SEC stated in Table 7, the overall energy consumption within the material processing phases is reduced by 34 MJ with varying the OF from 1 Hz to 4.5 Hz. The additional energy consumption of 6.5 kJ caused by the robot system is therefore neglectable.

If the increase in SEC from Table 8 is divided by 11 cm of the length of the measured wall, the following

relationship results: for a 10cm high wall, with an oscillating amplitude of 6 mm and 12 m/min wire feed speed, 3.1 MJ SEC can be saved for every centimeter wall length if an OF of 4.5 Hz is used instead of 1 Hz.

Table 8: Conversion of the saved chip volume into SEC.

OF [Hz]	Machined mass for both wall sides [g]	Increase of machined mass relative to 4.5 Hz [g]	Increase in SEC for material processing relative to 4.5 Hz [MJ]
1	110	53	34
2.5	67	10	6.4
4.5	57	-	-

In principle, however, the produced chips can be recycled and a saving in primary material production is therefore possible. This would have to be considered for a final evaluation of the SEC and the used OF. Due to a lack of values for such savings through recycled material, this has not been done at this point. However, it is assumed that the result does not change fundamentally, but that the difference is merely smaller.

4. Summary and conclusion

In this paper, the influence of different oscillation frequencies using a DED-Arc process on the resulting surface of an additively manufactured Ti-6Al-4V wall was investigated. In addition to the description of the surface, the conversion of the resulting machining volume into a SEC was a key feature for evaluating the results. The following conclusions were drawn:

- Increasing oscillation frequency within the process limits leads to an improved surface with reduced tread depth and roughness.
- The volume to be machined decreases with increasing oscillation frequency and is halved from 1 Hz to 4.5 Hz, resulting in a significant saving in SEC.
- The differences in the values for the surface profile and chip removal rate are greatest between 1 Hz and 2.5 Hz. A further increase of the OF to 4.5 Hz brings a further improvement in any consideration, but the relative improvement decreases sharply.
- An increasing oscillation frequency results in higher energy consumption of the robot. In relation to the presented application, the value is lower by a factor of 1000, rendering the additional effort negligible.

- When using 4.5 Hz instead of 1 Hz, each cm of a 10 cm high wall results in SEC savings of 3.1 MJ.

5. Outlook

From the point of view of the surface quality and SEC, there is a clear recommendation for choosing the optimum OF for the DED-Arc process. However, it would also be necessary to examine what other effects result from a changed OF. The increased movement sequence and speed may result in increased wear of certain parts, e.g. the current contact tube. On the other hand, a high OF could lead to more uniform cooling or a changed cooling rate with positive effects for the mechanical properties. Furthermore, it would be interesting to compare it with the meander strategy, which is widely used in the state of the art and to verify whether the advantages demonstrated here can be transferred to that strategy. Additionally, it should be examined whether the effect can also be transferred to other materials, although the advantage is greatest for materials with high energy requirements for raw material production such as titanium.

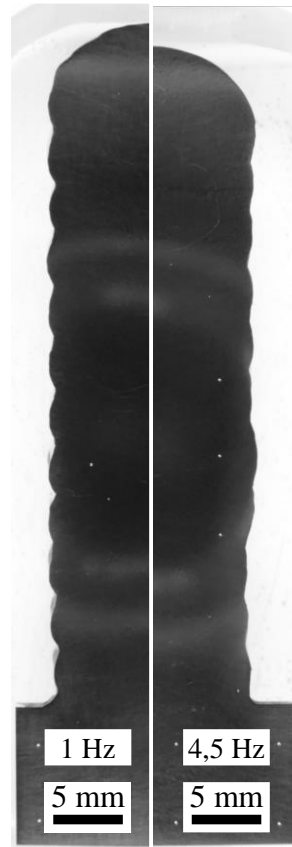


Figure 7: Comparison of two micrographs with different OF from preliminary tests and hardness imprints.

6. Acknowledgement

The authors express their sincere thanks to the Federal Ministry of Economics and Climate Protection and the German Aerospace Center for providing funding and support for the associated project.

7. Annex



Figure 6: Visualization of the upper process limit due to a centrally split weld seam caused by excessively fast torch movements.

– References

- [1] BUSINESS WIRE, *Norsk Titanium to Deliver the World's First FAA-Approved, 3D-Printed, Structural Titanium Components to Boeing: Boeing 787 Dreamliner will be First Commercial Airplane to Fly with Certified Additive-Manufactured Titanium Parts in Structural Applications.* [Online]. Available: <https://www.businesswire.com/news/home/2017041005330/en/Norsk-Titanium-to-Deliver-the-World's-First-FAA-Approved-3D-Printed-Structural-Titanium-Components-to-Boeing> (accessed: March 22nd 2024).
- [2] T. A. Rodrigues, V. Duarte, R. M. Miranda, T. G. Santos, and J. P. Oliveira, "Current Status and Perspectives on Wire and Arc Additive Manufacturing (WAAM)," *Materials (Basel, Switzerland)*, vol. 12, no. 7, 2019, doi: 10.3390/ma12071121.
- [3] A. C.M. Bekker and J. C. Verlinden, "Life cycle assessment of wire + arc additive manufacturing compared to green sand casting and CNC milling in stainless steel," *Journal of Cleaner Production*, vol. 177, pp. 12–040, pp. 438–447, 2018, doi: 10.1016/j.jclepro.2017.12.148.
- [4] I. H. Shah, N. Hadjipantelis, L. Walter, R. J. Myers, and L. Gardner, "Environmental life cycle assessment of wire arc additively manufactured steel structural components," *Journal of Cleaner Production*, vol. 389, no. 2, p. 136071, 2023, doi: 10.1016/j.jclepro.2023.136071.
- [5] P. C. Priarone, E. Pagone, F. Martina, A. R. Catalano, and L. Settineri, "Multi-criteria environmental and economic impact assessment of wire arc additive manufacturing," *CIRP Annals*, vol. 69, no. 1, pp. 37–40, 2020, doi: 10.1016/j.cirp.2020.04.010.
- [6] R. C. Reis, S. Kokare, J. P. Oliveira, J. C.O. Matias, and R. Godina, "Life cycle assessment of metal products: A comparison between wire arc additive manufacturing and CNC milling," *Advances in Industrial and Manufacturing Engineering*, vol. 6, no. 3, p. 100117, 2023, doi: 10.1016/j.aime.2023.100117.
- [7] S. Kokare, J. P. Oliveira, and R. Godina, "Life cycle assessment of additive manufacturing processes: A review," *Journal of Manufacturing Systems*, vol. 68, pp. 536–559, 2023, doi: 10.1016/j.jmsy.2023.05.007.
- [8] S. Kokare, J. P. Oliveira, T. G. Santos, and R. Godina, "Environmental and economic assessment of a steel wall fabricated by wire-based directed energy deposition," *Additive Manufacturing*, vol. 61, p. 103316, 2023, doi: 10.1016/j.addma.2022.103316.
- [9] P. C. Priarone, G. Campatelli, F. Montevicchi, G. Venturini, and L. Settineri, "A modelling framework for comparing the environmental and economic performance of WAAM-based integrated manufacturing and machining," *CIRP Annals*, vol. 68, no. 1, pp. 37–40, 2019, doi: 10.1016/j.cirp.2019.04.005.
- [10] J. González, I. Rodríguez, J.-L. Prado-Cerqueira, J. L. Diéguez, and A. Pereira, "Additive manufacturing with GMAW welding and CMT technology," *Procedia Manufacturing*, vol. 13, no. 4, pp. 840–847, 2017, doi: 10.1016/j.promfg.2017.09.189.
- [11] L. Vázquez, N. Rodríguez, I. Rodríguez, E. Alberdi, and P. Álvarez, "Influence of interpass cooling conditions on microstructure and tensile properties of Ti-6Al-4V parts manufactured by WAAM," *Weld World*, vol. 64, no. 8, pp. 1377–1388, 2020, doi: 10.1007/s40194-020-00921-3.
- [12] S. W. Williams, F. Martina, A. C. Addison, J. Ding, G. Pardal, and P. Colegrove, "Wire + Arc Additive Manufacturing," *Materials Science and Technology*, vol. 32, no. 7, pp. 641–647, 2016, doi: 10.1179/1743284715Y.0000000073.
- [13] T. ABE and H. SASAHARA, "Simulating the build shape for a shell structure for wire and arc additive manufacturing using the bead cross-section model," *Journal of Advanced Mechanical Design, Systems, and Manufacturing*, vol. 15, no. 1, 2021, doi: 10.1299/jamdsm.2021jamdsm0001.
- [14] S. A. Banaee, A. Kapil, F. Marefat, and A. Sharma, "Generalised overlapping model for multi-material wire arc additive manufacturing (WAAM)," *Virtual and Physical Prototyping*, vol. 18, no. 1, 2023, doi: 10.1080/17452759.2023.2210541.
- [15] M. S. Mohebbi, M. Kühn, and V. Ploshikhin, "A thermo-capillary-gravity model for geometrical analysis of single-bead wire and arc additive manufacturing (WAAM)," *The International Journal of Advanced Manufacturing Technology*, vol. 109, 3-4, pp. 877–891, 2020, doi: 10.1007/s00170-020-05647-6.
- [16] W. Zhang, C. Ding, H. Wang, W. Meng, Z. Xu, and J. Wang, "The Forming Profile Model for Cold Metal Transfer and Plasma Wire-Arc Deposition of Nickel-Based Alloy," *Journal of Materials Engineering and Performance*, vol. 30, no. 7, pp. 4872–4881, 2021, doi: 10.1007/s11665-021-05485-x.
- [17] J. Fu *et al.*, "Effect of Tool-Path on Morphology and Mechanical Properties of Ti-6Al-4V Fabricated by Wire and Arc Additive Manufacturing," *MATEC Web Conf.*, vol. 128, p. 5009, 2017, doi: 10.1051/mateconf/201712805009.
- [18] T. H. Lee, D. H. Kam, J. H. Oh, and C. Kim, "Ti-6Al-4V alloy deposition characteristics at electrode-negative polarity in the cold metal transfer-gas metal arc process," *Journal of Materials Research and Technology*, vol. 19, no. 5, pp. 685–696, 2022, doi: 10.1016/j.jmrt.2022.05.030.
- [19] A. K. Syed *et al.*, "Effect of deposition strategies on fatigue crack growth behaviour of wire + arc additive manufactured titanium alloy Ti-6Al-4V," *Materials Science and Engineering: A*, vol. 814, p. 141194, 2021, doi: 10.1016/j.msea.2021.141194.
- [20] E. Farabi, T. Klein, M. Schnall, and S. Primig, "Effects of high deposition rate during cold metal transfer additive manufacturing on microstructure and properties of Ti-6Al-4V," *Additive Manufacturing*, vol. 71, p. 103592, 2023, doi: 10.1016/j.addma.2023.103592.
- [21] J. Gou *et al.*, "Effects of trace Nb addition on microstructure and properties of Ti-6Al-4V thin-wall

- structure prepared via cold metal transfer additive manufacturing," *Journal of Alloys and Compounds*, vol. 829, no. 1, p. 154481, 2020, doi: 10.1016/j.jallcom.2020.154481.
- [22] P.-l. Zhang *et al.*, "Effect of deposition rate on microstructure and mechanical properties of wire arc additive manufacturing of Ti-6Al-4V components," *J. Cent. South Univ.*, vol. 28, no. 4, pp. 1100–1110, 2021, doi: 10.1007/s11771-021-4683-0.
- [23] C. Halisch, C. Gaßmann, and T. Seefeld, "Investigating the Reproducibility of the Wire Arc Additive Manufacturing Process," *AMR*, vol. 1161, pp. 95–104, 2021, doi: 10.4028/www.scientific.net/AMR.1161.95.
- [24] C. Halisch, B. Milcke, T. Radel, R. Rentsch, and T. Seefeld, "Influence of oxygen content in the shielding gas chamber on mechanical properties and macroscopic structure of Ti-6Al-4V during wire arc additive manufacturing," *Int J Adv Manuf Technol*, vol. 124, 3-4, pp. 1065–1076, 2023, doi: 10.1007/s00170-022-10214-2.
- [25] L. Mashigo, H. Möller, and C. Gassmann, "Comparison of the mechanical properties of Grade 5 and Grade 23 Ti6Al4V for wire-arc additive manufacturing," *Journal of the Southern African Institute of Mining and Metallurgy*, vol. 121, no. 7, pp. 325–330, 2021, doi: 10.17159/2411-9717/1498/2021.
- [26] *Geometrische Produktspezifikation (GPS) – Oberflächenbeschaffenheit: Profile – Teil 3: Spezifikationsoperatoren (ISO 21920-3:2021); Deutsche Fassung EN ISO 21920-3:2022*, DIN EN ISO 21920-3, DIN Deutsches Institut für Normung e. V., Berlin, Dec. 2022.
- [27] P. C. Priarone, G. Ingarao, R. Di Lorenzo, and L. Settineri, "Influence of Material-Related Aspects of Additive and Subtractive Ti-6Al-4V Manufacturing on Energy Demand and Carbon Dioxide Emissions," *J of Industrial Ecology*, vol. 21, S1, p. 30, 2017, doi: 10.1111/jiec.12523.
- [28] R. Lyons, A. Newell, P. Ghadimi, and N. Papakostas, "Environmental impacts of conventional and additive manufacturing for the production of Ti-6Al-4V knee implant: a life cycle approach," *Int J Adv Manuf Technol*, vol. 112, 3-4, pp. 787–801, 2021, doi: 10.1007/s00170-020-06367-7.
- [29] T. D. Ngo, A. Kashani, G. Imbalzano, K. T.Q. Nguyen, and D. Hui, "Additive manufacturing (3D printing): A review of materials, methods, applications and challenges," *Composites Part B: Engineering*, vol. 143, no. 2, pp. 172–196, 2018, doi: 10.1016/j.compositesb.2018.02.012.
- [30] S. Ehmsen, L. Yi, and J. C. Aurich, "Process Chain Analysis of Directed Energy Deposition: Energy flows and their influencing factors," *Procedia CIRP*, vol. 98, pp. 607–612, 2021, doi: 10.1016/j.procir.2021.01.162.
- [31] AMPOWER GmbH & Co. KG, *Specific Energy Calculator*: AMPOWER GmbH & Co. KG, 2023.